RSC Advances

PAPER

View Article Online
View Journal | View Issue

Cite this: *RSC Adv.*, 2026, **16**, 25024

Hydrogel nanoparticle synthesis using liquid–solid separation for a more efficient, greener process

Emily N. Ingram, Jason Stallings, Jr, Mara Leach-Baughman, Endras Fadhilah, Anastasia Shaverina, Brittany E. Givens and Malgorzata Chwatko *

Water swollen nanoparticle synthesis methods have been fine-tuned and universally used to create materials in the medical and cosmetic industries. However, these methods often utilize toxic solvents and generate excess waste during the separation and purification processes. This work presents a protocol using an inverse nanoemulsion wherein liquid–liquid separation is replaced with liquid–solid separation, *i.e.* crystallization to isolate nanoparticles. Using low toxicity oils that are solids at room temperature, water-in-oil nanoemulsions can be generated at elevated temperatures, and upon removal of heat, solid–liquid separation isolates nanoparticles in the aqueous phase. Poly(ethylene glycol) diacrylate (PEG-DA) was chosen to create polymer nanogels *via* thermally induced radical polymerization and redox polymerization. Myristic acid inverse nanoemulsions with two molecular weights of PEG-DA (M_n = 8000 and M_n = 575) and two different stirring speeds were initially used to evaluate the system dynamics, particle size, and recovery. Scanning electron microscopy was used to evaluate the average particle size of 195.8 ± 99.95 nm for PEG-DA(8000) at 100 rpm and 208.7 ± 144.1 nm for PEG-DA(575) at 100 rpm. Myristic acid was successfully recycled to synthesize additional PEG-DA(575) based particles, achieving a consistent particle size. The sustainability of the process was evaluated using the *E*-factor and process mass intensity for the individual recycling steps and the overall process from the beginning to the end of life. An average *E*-factor of 19.7 ± 5.5 and an average process mass intensity of 173.4 ± 56.1 were determined in the presented method with oil recycling stages. Finally, lipase from porcine pancreas was encapsulated in the synthesized nanoparticles to demonstrate the versatility of the method and ability to generate particles with low thermal stability cargo. By extending the recrystallization strategy to nanoparticle synthesis, a vast improvement in the sustainability of nanoparticle synthesis compared to commonly used techniques was determined. This study paves the way for other researchers to adopt sustainable synthesis strategies with other water-soluble monomers or macromers.

Received 9th October 2025
Accepted 5th May 2026

DOI: 10.1039/d5ra07694c

rsc.li/rsc-advances

Introduction

The push towards green chemistry and engineering is becoming more popular as policies, regulations, and public opinion are shifting. Nanotechnology and nanomedicine are not spared from the increased scrutiny of using toxic or environmentally hazardous materials. The movement towards safer nanoparticles includes careful analysis of the reagents and methods used to synthesize them. During nanoparticle synthesis, sustainability is greatly affected by the amount of waste generated, use of toxic organic solvents, and the number of purification cycles required.[1–3] As noted by Najahi-Missaoui, in 2019, less than 17% of the nanoparticle publications mentioned safety or sustainability, which highlights the sustainability gap that needs to be addressed in future studies.[4–7] Expansion of the key word search to 2024 showed that publications on nanoparticle safety, in terms of toxicity and human usage, increased to 34% of the total number of nanoparticle publications in 2024, compared to 15% in 2000, as shown in Fig. 1. However, when accounting for sustainability and greener processes, only 25% of the total nanoparticle publications mentioned these keywords. Therefore, rethinking the design of nanoparticle synthesis, including the solvents and methods of fabrication and purification, can lead to safer nanoparticles for both environmental and commercial usage.

Nanogels and microgels are hydrogel-based nanoparticles with high water content and large surface-area-to-bulk volume ratio. Due to these features, nanogels are often used to encapsulate and deliver active ingredients, thereby allowing for longer blood circulation time of protected active ingredients *versus* direct injection.[8,9] The biocompatibility and degradability of the materials composing the particles are essential for their safe use in the human body.[10] Poly(ethylene glycol) (PEG) is a common polymer used in pharmaceutical agents, as it is a hydrophilic polymer that is generally considered non-toxic *in vivo*.[8,9] PEG is

Chemical and Materials Engineering Department, Pigman College of Engineering, University of Kentucky, Lexington, KY, USA. E-mail: m.chwatko@uky.edu

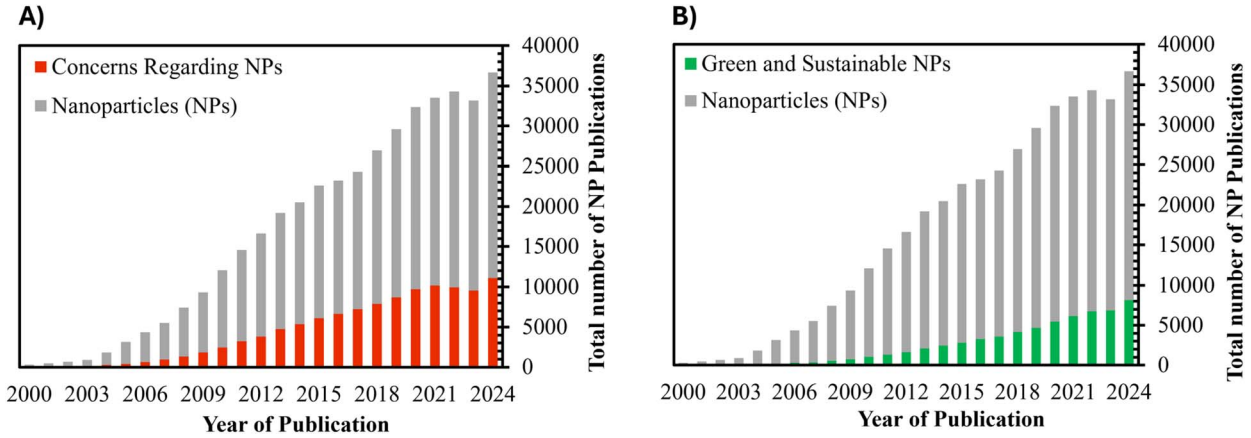

Fig. 1 (A) The number of articles expressing concern regarding nanoparticle use (red) out of all articles discussing nanoparticles. (B) The number of articles expressing sustainability or green chemistry in nanoparticle use (green) out of all articles discussing nanoparticles.

not an easily biodegradable polymer nonetheless when PEG particles are synthesized the structure can be crosslinked with functional end groups such as dithiols and acrylates to serve as degradable linkers in the formed network.[11–14] Smaller PEG chains can be removed from the body through the kidneys.[15,16]

Nano- and micro-gels can be constructed using a water-in-oil (W/O) emulsification technique, where water soluble monomers are dispersed in water droplets in a continuous oil medium.[17] Using PEG-DA as a monomer, in the presence of an initiator, a crosslinked network in the shape of the water droplet is formed. In W/O emulsions, the stability of the droplets is imperative for creating nano/microgels of similar particle sizes and efficiently purifying the particles. Ostwald ripening has been studied by using oils such as heptane, decane, and dodecane as the continuous phase and stabilized using an emulsifier.[18] It was discovered that as the hydrocarbon chain increases, the rate of Ostwald ripening decreases because there is an increase in the hydrophobicity of the continuous phase. In addition, as the hydrocarbon chain increases, the viscosity of the continuous phase has also been shown to play a substantial role in the stability of droplets.[19] Furthermore, the usage of surfactants can reduce surface tension of the droplets, decreasing the rate of flocculation and coalescence. However, surfactants are not cost-effective for scaling up, can cause irritation when used in personal care products and also increase associated waste production.[20–23] Not only does the stability of the droplets contribute to particle size, nano/microgels size can also be controlled by varying the molecular weight, the distance between polymer crosslinks and stirring speed.[24,25]

After polymerization occurs, the nano/microgels can be isolated using various techniques such as solvent evaporation, salting out, and dialysis.[26,27] In recent years, improvements in the sustainability of the emulsion process include the movement away from petrochemical solvents, such as heptane discussed above, to those that are naturally derived, such as plants and vegetable oils.[28–30] However, alternative methods for the removal of naturally derived oils to purify the nano/microgels are still lacking. Abdel-Raouf, *et al.* created polyacrylamide-guar gum hydrogels using free radical polymerization. The guar gum hydrogel particles swollen with distilled water were precipitated out using excess acetone and washed with large amounts of methanol. An ideal purification method would include only the usage of water to wash excess oil from the dispersant phase and reduce the number of washes required. Therefore, there is a universal need for an improvement of well-established emulsion techniques for the reduction of the waste generated and the use of toxic solvents for purification of nanoparticles.[31–33]

Crystallization is an alternative technique often used in organic chemistry, to increase the purity of chemicals from contaminants with alternate solubilities.[34] In the case of crystalline molecules such as lactide, crystallization can be employed to reach high-purity materials.[35] Considering traditional emulsions, both phases are typically liquids at room temperature, therefore for isolation of particles, liquid–liquid separation is required for non-volatile solutions, often involving several washing steps, and ultimately precipitation or centrifugation leading to larger amounts of waste. However, with the push towards greener and more sustainable materials, the incorporation of oils, such as fatty acids, which are capable of crystallization can be used to enable solid–liquid phase separation.

In this work, an alternative strategy for the synthesis of hydrogel nanoparticles, namely PEG, using a water-in-oil emulsion by recrystallization of the continuous phase is described. Saturated fatty acids were used as a continuous phase due to their relatively low crystallization temperature. The effect of increasing stirring speed and monomer molecular weight on the purified nano/microgel particle size and recovery was investigated. To increase the overall sustainability of the method, the recyclability of the continuous phase was explored, and the impacts on particle size and yield were investigated. To highlight the versatility of the method to less thermally stable species, such as lipase enzymes, a redox initiator based method was explored. Lastly, sustainability parameters, Process Mass Index (PMI) and *E*-factor, were used to evaluate the greenness of

the proposed solid–liquid synthesis and purification method described. The successful synthesis of nanogels while ensuring low sustainability metrics in this method highlights the opportunities for more sustainable nanogel synthesis approaches.

Results and discussion

Methodology development

Water-in-oil emulsions have been used extensively to create hydrogel nanoparticles. However, the purification methods often require excess solvents to bring the two-phase system into a single-phase solution. In addition, not all solvents utilized in this process can be classified as green solvents; this is often the case when the purification method requires solvent evaporation. To address this, crystallization was evaluated to simplify the purification strategies by utilizing a solid–liquid phase separation. While many molecules can crystalize at temperatures between 30–90 °C, saturated fatty acids provide the use of sustainably sourced and lower toxicity compounds. Additionally, saturated molecules ensure there is no cross-reactivity or unwanted side reactions with the oil phase. Generally, fatty acids are also considered to be a poor solvent for many hydrophilic monomers and macromers, such as PEG which prefer the aqueous phase.[36] This enables fatty acids to be an effective non-solvent for hydrogel particle synthesis.

The project methodology design is illustrated in Scheme 1 where an oil was used as the continuous phase at an elevated temperature of 70 °C, and the aqueous phase, containing our macromer and initiator was the disparate phase. Stirring was used to emulsify, and the stirring speed was controlled using a stir plate. After the reaction, the phase separation of oil and water happens quickly due to the absence of an emulsifier, and oil solidification is dependent on its crystallization temperature and cooling rate. To ensure a higher nanogel yield, additional water was added before the oil phase solidification. While not investigated, centrifugation prior to cooling may also increase yields. Upon cooling, the oil can be simply removed from the top of the vessel due to its lower density than water. Often, some smaller oil particles were found in the water phase. To remove these particles, vacuum filtration and syringe filtration were implemented before lyophilization of the aqueous layer. For macromers which are more miscible within the oil phase, the oil may get trapped in the particle network or the macromer may diffuse to the oil layer. These more oleophilic particles require additional washing.

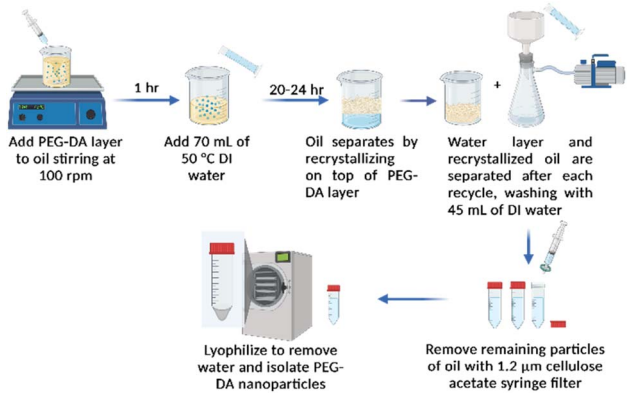

Scheme 1 Process design for synthesizing hydrogel nanoparticles with a water-in-oil nanoemulsion.

Commonly, emulsions use emulsifiers to reduce the interfacial tension, preventing coalescence and improving the kinetics stability of the particles.[21,37–39] Our technique does not call for the usage of emulsifiers, relying on the hydrophilicity of PEG-DA and the slight emulsifying property of the fatty acids.[33] In addition, as the continuous phase is more viscous, the droplets are less likely to grow by coalescence.[40] Akram *et al.* studied the effect of six different oils on droplet size, finding there was little variation in the diameter of droplets formed, and as such the our method ultimately did not use emulsifiers.[21,31,37–39]

Varying stirring speed with PEG-DA(8000)

PEG-DA nanogels were synthesized using a W/O nanoemulsion with stirring speeds of 100 and 900 rpm and isolated from the water phase utilizing freeze drying. The recovery for PEG-DA(8000) was 7.13 ± 3.8% for 100 rpm and 16.70 ± 11.9% for 900 rpm, using eqn (1). The low recovery for both stirring speeds may be due to some particles being still trapped in the oil layer from either incomplete phase separation or losses during the filtration stages in the purification. The particle sizes were analyzed after syringe filtering. The hydrodynamic diameter was 193.1 ± 87.8 nm for stirring speed of 100 rpm, and 149.6 ± 83.2 nm for a stirring speed of 900 rpm, as seen in Fig. 2. As suspected, the increase in stirring speed slightly decreased the particle size, albeit not statistically significant, due to an increase in shear and additional breakup of droplets. Similar trends were identified by Niknam *et al.*, which presents the stability of W/O droplets by developing an optimal method to create nano-emulsions using Mygylol 812 as an alternative oil phase. Their droplet sizes ranged from 105.8 ± 10.3 nm at 20 000 rpm to 286.9 ± 15.2 at 11 000 rpm. They also found that at higher stirring speed, smaller droplets led to more stable emulsions over time. Similarly, other studies at lower stirring speed also found that size decreased upon an increase in shearing due to the improvement in the homogeneity of water spreading into the oil.[41–44]

In addition to DLS, particles were characterized using SEM and the results can be seen in Fig. 2. The results confirm that the particles are larger for a stirring speed of 100 rpm with the average particle sizes of 195.80 ± 99.95 nm and 72.11 ± 20.55 nm for 900 rpm. As aforementioned, previous studies have shown that higher stirring speeds lead to smaller droplet sizes with more stable emulsions, thus reducing the dispersity of particle sizes throughout. With a decrease in stirring, or decrease in shear forces, the droplets have a higher tendency to coalesce, leading to greater dispersity in droplet sizes. In addition, due to the higher viscosity of the aqueous phase when using PEG-DA(8000), it is possible that the droplets are not sheared to their minimum size before polymerization starts and

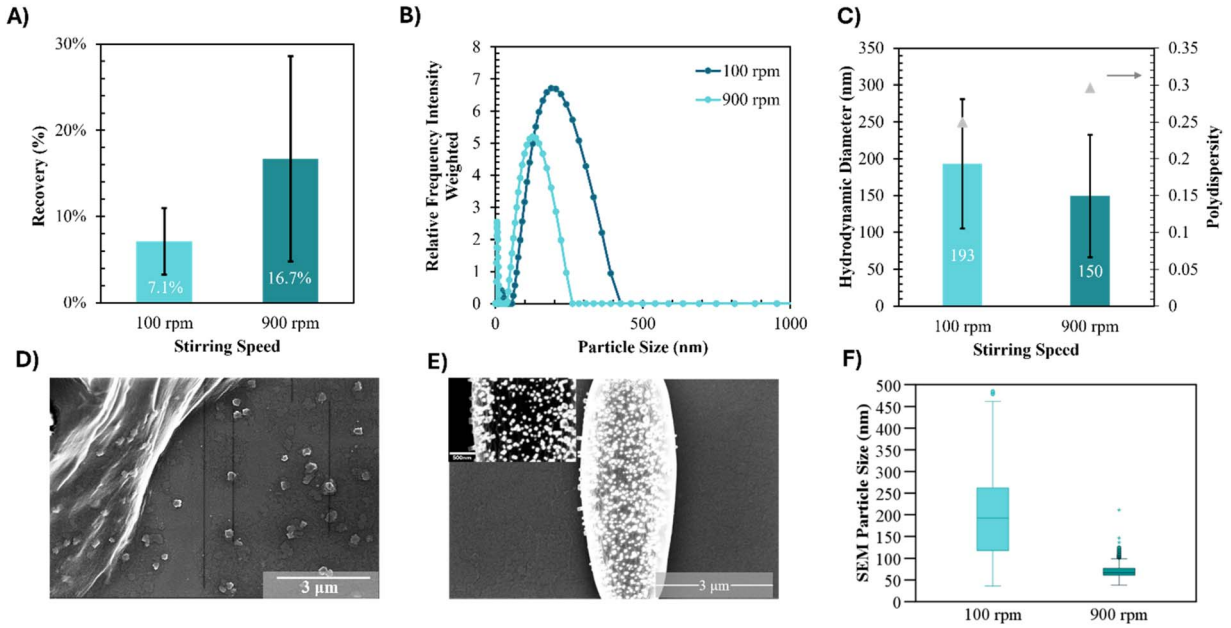

Fig. 2 (A) Recovery of PEG-DA(8000) nanoparticles at different stir speeds was determined gravimetrically ($n = 3$). Two-tailed Student's t-test analyzed statistical significance, $t(4)$ $p = 0.225$. (B) Representative dynamic light scattering (DLS) curve of PEG-DA(8000) post syringe filtration within 2 hours of synthesis. (C) Hydrodynamic diameter of synthesized nanogels from PEG-DA(8000) at 100 and 900 rpm ($n = 3$) and 900 rpm ($n = 2$), was 193.1 ± 87.8 and 149.6 ± 83.2 nm, respectively. Polydispersity was 0.29 ± 0.03 and 0.25 ± 0.02 for 100 and 900 rpm, respectively. The samples were analyzed post syringe filtration within 2 hours of synthesis. (D) Scanning electron microscopy (SEM) images for dry PEG-DA(8000) particles at 100 rpm ($n = 200$, $N = 2$). The large sheet defect is hypothesized to be myristic acid left over in the sample. (E) Scanning electron microscopy (SEM) images of dry PEG-DA(8000) at 900 rpm ($n = 100$, $N = 2$). Individual particles are concentrated on the center of the image. (F) Size distribution of PEGDA particles at 100 rpm (aqua) and 900 rpm (teal) from SEM analysis. ($t(198)$, $p < 0.001$).

as such results in samples with large size variability. These sizes are smaller in comparison to those seen in DLS results due to a difference in hydration. As seen in Fig. 2F, the particle size distribution has a larger variance in the particle size for 100 rpm *versus* 900 rpm. It has been shown that mechanical energy plays a significant role in the break-up of particles in a liquid–liquid system.[33] With higher mechanical energy, in this case at higher stirring speeds, the interfacial tension lowers, allowing the drops to break apart more effortlessly, resulting in smaller particles as noted above. From the SEM images, particles stirred at 900 rpm are more spherical, with an increase in homogeneity in the solution. Previous studies investigated how particle sizes below and above a critical stirring speed were affected.[33]

Ohnesorge number describes the ratio of viscous forces to inertial and surface tension, serving as a good predictor of particle size. In addition, critical Weber number provides a measure of when droplet breakup occurs. Both values can be beneficial to explain why even at low shear rates, particles below 300 nm are obtained. To capture both values in nanoemulsion, Gupta *et al.* proposed a scaling factor using a ratio of the continuous and disparate phase viscosity, related to both Ohnesorge number and Weber number.[45] In the emulsion system presented in the study, there is a significant difference in disparate *vs.* continuous phase viscosity. This ensures that the disparate phase is easier to break up, and the continuous phase viscosity prevents rapid coalescence. Using eqn (5), the viscosity scaling factor was approximately 0.3, which based on work Gupta *et al.*, predicts the creation of small droplets below 100 nm.

Impact of varying macromer molecular weight

To determine the technique's sensitivity to macromer size, a smaller molecular weight PEG-DA(575) was tested. DLS indicated a similar trend with stirring speed as PEG-DA(8000), as seen in Fig. 3. The SEM analysis showed similar particle sizes, below 500 nm; however, stirring speed did not impact particle size. This loss of sensitivity is attributed to a purity issue as the particles appear to have changes in their physical properties due to a higher oil miscibility with PEG-DA(575) than PEG-DA(8000).

To investigate the purity of the resulting nanoparticle samples, NMR spectroscopy and HPLC were utilized. As seen in Fig. 3, there was a strong singlet peak at 1.56 ppm indicative of the methyl group ($-CH_3$) in myristic acid. The presence of myristic acid in these samples help explain an occasional peak above 1.2 µm observed in the DLS which should not be possible after syringe filtration. Previous studies using PEG-DA at different molecular weights found that lower molecular weight PEGs have a lower water solubility.[32] The increase in hydrophilicity of PEG-DA(8000) decreases the partitioning of oil into the particles in the water layer. However, the purity information found in the study noted only a minor contamination from myristic acid with purity greater than 99%. NMR purity notes incomplete reaction of PEG-DA and as such drops the purity to 97%. To obtain SEM images without myristic acid

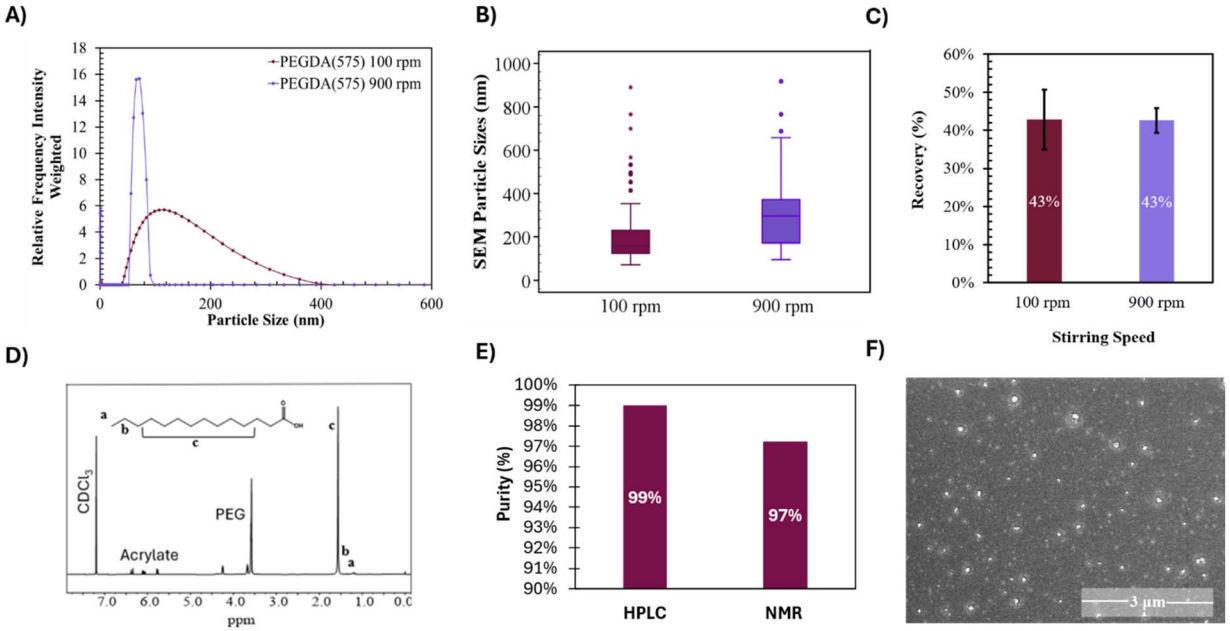

Fig. 3 (A) Representative DLS data of particles PEG-DA(575) stirring at 100 rpm (maroon) and 900 rpm (lilac) resuspended for over twenty-four hours (B) dry particle sizes and the distribution from SEM analysis using ImageJ of PEG-DA(575) stirring at 100 rpm (maroon) and 900 rpm (lilac). The average size for PEG-DA(575) 100 rpm was observed to be 208.7 ± 144.11 nm, and 310.09 ± 166.89 nm for 900 rpm. ($t(198)$, $p < 0.001$). (C) Recovery of PEG-DA(575) particles at 100 rpm were calculated to be 42.8% ± 0.1, and 42.7% ± 0.03 at 900 rpm ($n = 3$). This recovery shows good reproducibility, even with the increase in stirring speed. ($t(2)$, $p = 0.97$). (D) ^{1}H NMR in deuterated chloroform showed myristic acid presence in dried nanoparticles. (E) Purity of nanoparticles formed with PEG-DA(575) at 100 rpm stirring. HPLC purity considered myristic acid, NMR analysis considered myristic acid and unreacted PEGDA. (F) SEM image of dry PEG-DA(575) at 900 rpm.

contamination, six washes of particles with ethanol were performed. Lastly, the recovery of particles did not vary with stirring speed but was significantly higher than those obtained with PEG-DA(8000). We hypothesized that the increase in recovery may be due to the tighter network formed by PEG-DA(575) which may facilitate the phase separation into the water layer *versus* the highly water swollen higher molecular weight PEG macromer. The lower recovery of particles is likely not due to loss during filtration as particles have a diameter smaller than the pore size used in purification.

Impact of initiation mechanism

Another critical aspect of nanogel synthesis *via* polymerization is the method of reaction initiation. Thermal initiators provide a high degree of control over the initiation process, as elevated temperature is needed to create radicals. For reactants or cargo which are not thermally stable, a lower temperature mechanism may be needed. To achieve synthesis at a lower temperature myristic acid was replaced with capric acid, a C_{10} fatty acid, which has a melting point between 29–32.3 °C.[46,47] There have been several articles citing the usage of capric acid as either the oil phase in an emulsion or in a mixture with other oils such as lauric acid and caprylic acid.[31,48–50]

Redox based initiation process offers a pathway to reaction initiation at any temperature as long as the right pair of compounds is chosen. In this study, redox initiators, iron gluconate, and ammonium persulfate were chosen. This redox system showcases a lower safety risk *versus* the more common TEMED/APS combination.[51–56] To perform a comparison study on the initiation method, thermal and redox initiator system were used at the same elevated temperature. Fig. 4 shows the diameter of the nanogels in solution and while dry. The hydrated dataset did not show any differences in size between polymers as shown by DLS. Redox samples had a slightly lower particle diameter identified by SEM measurements also shown in Fig. 4. This difference is significant, but it has a small effect size. The potential smaller size could be due to a faster reaction time associated with the redox initiator which would limit particle coalescence or Oswald ripening.[46] The nanogel recovery was comparable across the samples, supporting that the initiator did not impact the phase separation of nanogels into the aqueous phase.

Impact of polymer type

To showcase method variability with additional water-soluble monomers or macromers, gelatin acrylate was used to create nanogels. Nanogels were synthesized utilizing solid–liquid separation using myristic acid as the oil phase. The average recovery of gelatin nanogels was 33.70% ± 21.58%. The lower recovery *vs.* PEG-DA(575) may be due to partial reaction of gelatin acrylate prior to myristic acid addition due to the higher temperature needed for full gelatin solubility. The particle sizes were similar to those used with PEG-DA due to the high interfacial tension between the oil and water layer, resulting in a stable emulsion. DLS and SEM were used to analyze the size of the nanogels in swollen *versus* the dried samples. The hydrated

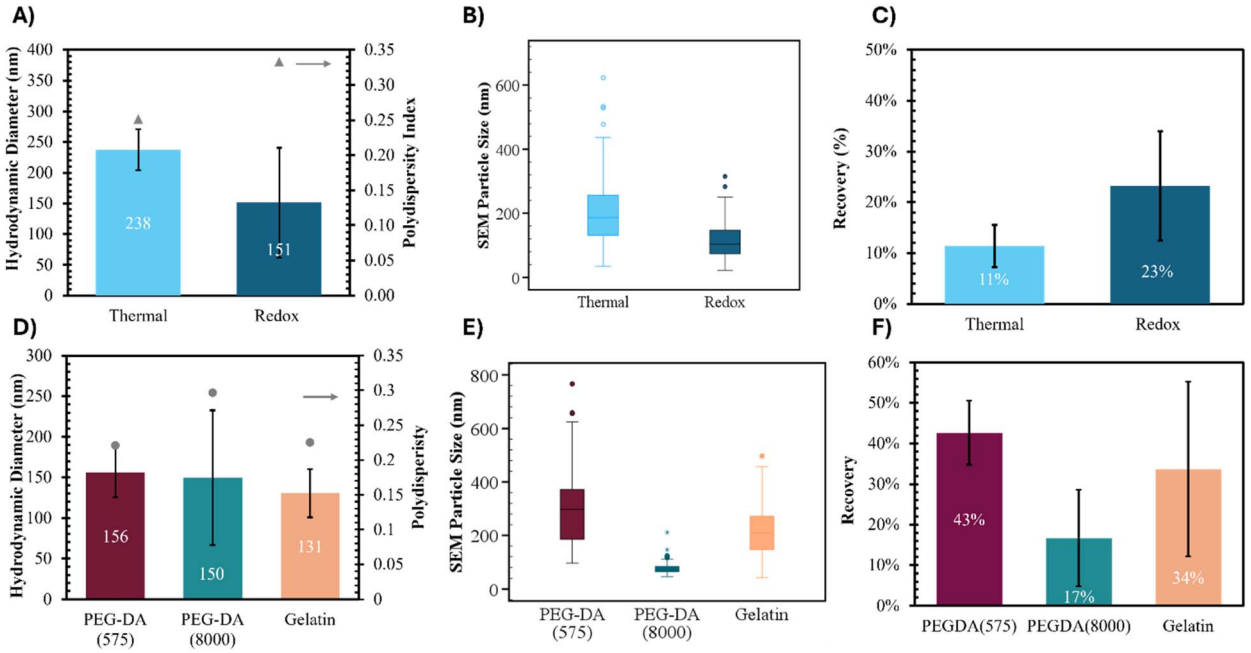

Fig. 4 (A) Hydrodynamic diameter for redox initiator ($n = 3$) and thermal initiator ($n = 2$), respectively for PEG-DA(575) stirred at 900 rpm. Polydispersity was 0.33 ± 0.15 and 0.25 ± 0.07 for redox and thermal initiator respectively. Both reactions were done at 70 °C in myristic acid. The samples were analyzed post syringe filtration within two hours of synthesis. ($t(4)$, $p = 0.3$) (B) particle sizes and the distribution from SEM analysis using ImageJ of dry PEG-DA(575) particles stirred at 900 rpm. ($n = 100$, $N = 2$ for redox, $n = 107$, $N = 2$ for thermal). ($t(206)$, $p < 0.001$). (C) Recovery of nanoparticles determined gravimetrically ($n = 3$). ($t(5)$, $p = 0.15$) (D) hydrodynamic diameter of different polymeric nanogels. The samples were analyzed post syringe filtration within two hours of synthesis. The reactions were done at 900 rpm at 70 °C in myristic acid ($n = 3$) (E) dry particle sizes and the distribution from SEM analysis using ImageJ. ($n = 100$, $N = 2$ PEG-DA(575); $n = 200$, $N = 2$ PEG-DA(8000); $n = 60$, $N = 2$ gelatin-acrylate) the effect size between gelatin and PEG-DA(575) was −0.37 ($t(160)$, $p < 0.0001$), using Cohen's d value and the standard deviations. Furthermore, the effect size between gelatin and PEG-DA(8000) was 0.7 ($t(81)$, $p < 0.0001$) (F) recovery of nanoparticles synthesized from different polymers determined gravimetrically ($n = 3$).

particles showed similar hydrodynamic diameter using DLS. The dried nanogels had the average particle diameter was 204.1 ± 91.95 nm, which fell in between the nanogels synthesized with high and low molecular weight PEG.

Other significant parameters

In any emulsion method, a variety of parameters can be adjusted to achieve different nanoparticle sizes and yields. These include factors like stirring speed, the type of macromer or monomer, as well as others such as the oil-to-water ratio, the viscosity of the continuous phase, and more. While not all variations of this method were tested, additional studies varying oil viscosity and ratio of oil to water are presented in the SI Fig. S5 and S6. Generally, parameters such as oil to water ratio did not play a significant role in the particle size but led to significant changes in the nanogel yield. Overall, the method demonstrated its effectiveness, as the adjustments resulted in only minor variations in nanoparticle recovery and size.

Lastly, the proposed sustainable method was also comparable to methods which utilize more traditional solvents/non-solvents such as heptane which is shown in SI Fig. S14. SEM analysis showed similar particle sizes, and size distributions, but higher recovery. While outside the scope of this work, if the size distribution is too large from the shear based processed studied in this work, other methods such as microfluidics or membranes can be utilized to lower the particle size distributions using the oils proposed in this work.[57,58]

Assessing sustainability metrics

In Fig. 5, a sustainability metric score was given to each sample by calculating the Process Mass Intensity (PMI) and *E*-factor which have been widely used to evaluate process design.[59–62] As the PMI approaches one and *E*-factor is closer to zero, the metrics indicate a more "green" process.[63] As seen in Fig. 5, the PMI for PEG-DA(575) 100 rpm samples has an average score of 227.84 ± 18.38, whereas, the score for the *E*-factor was 27.82 ± 2.24. Compared to other hydrogel synthesis techniques, our process' PMI is significantly lower, with a solvo-thermal base treatment used to create chitosan nanocrystals having a PMI of 441.8 and another similar technique reaching a PMI of 789.3.[64] The *E*-factor in our work matches the minimum range of most pharmaceutical processes, whose *E*-factors range from 25–100.[65] To better understand the process reagent breakdown, Fig. 5C highlights in detail the amounts of reagents used compared to the process waste. The process waste is calculated as the waste produced such as syringes and filters, for Trial 1 and 2 were 12.21% and 10.45%. These values were calculated by weighing the amount of waste produced from the process and divided by the PMI. Water constituted 63.62% and 54.47% of the amount of materials used compared to the process waste for Trial 1 and

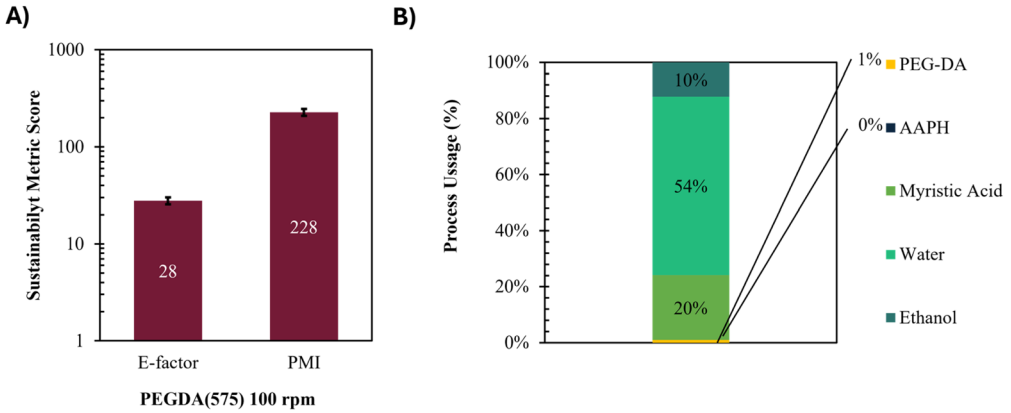

Fig. 5 (A) PMI and *E*-factor sustainability metric score of two PEG-DA(575) particles synthesized ($n = 3$). To further evaluate the waste and how much materials were being used during this process, (B) process use of material in PEG-DA(575) particle synthesis. The amount of materials used, in grams, and compares it to the total weight of materials used for the entire process $n = 3$.

Trial 2, respectively. These values vary due to slight variances in the recovered PEG-DA(575).

Myristic acid recycle study

The successful nanoparticle synthesis presented above relied on single-use reagents to achieve both particle synthesis and purification. However, as the oil layer is not reactive, it should mainly remain unchanged during the nanoparticle synthesis, which created an opportunity to further increase the process sustainability through oil recycling. To determine if oil phase recycling was feasible, three left-over oil phase samples were reused six times to create more nanoparticles. Fig. 6 shows the results of the myristic acid recycling. As expected, some variability in weight was noted during recycling which was attributed to the loss of some myristic acid to the aqueous layer. In these cases, the myristic acid was brought back to the original weight to maintain the desired oil-to-water ratio. Additionally, with each oil recycling, we note that approximately 50% of the synthesized particles remain in the oil phase without secondary extraction with additional washes. These particles can then be removed during subsequent recycling stages.

Fig. 6 shows the particle sizes from synthesis using pristine myristic acid (R0) up to six times used myristic acid (R6) for two oil samples. Fig. 6A and B provide the results of the DLS of one

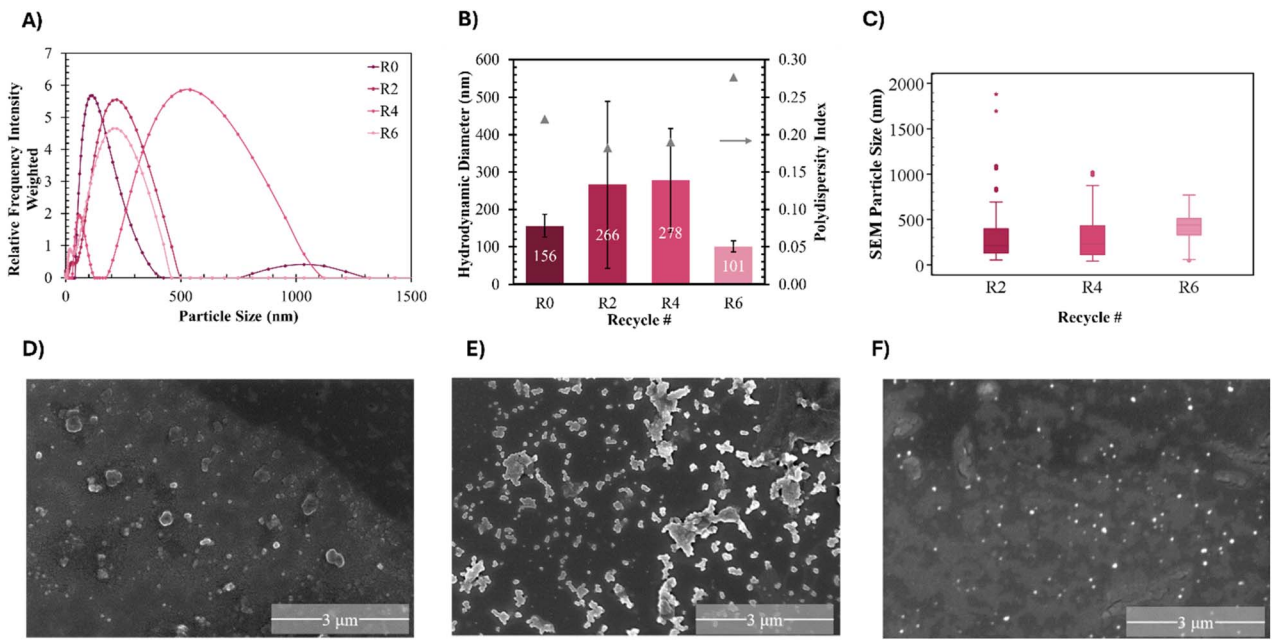

Fig. 6 Particles were made with myristic acid, 100 rpm, 70 °C thermal polymerization. (A) Particle size of PEG-DA(575) identified by DLS after recycling myristic acid up to six times and resuspended in DI water. The results represent a single trial of recycle loop. (B) The hydrodynamic diameter of PEG-DA(575) particles from select recycles ($n = 3$). (C) SEM results of dry particles PEG-DA(575) Trial 1 after recycling myristic acid two times ($n = 100$, $N = 2$), (D) SEM results of dry particles from trial 1, after recycling myristic acid two times (E) SEM results of dry particles from trial 1 after recycling myristic acid four times and (F) SEM results of dry particles from trial 1 after recycling myristic acid six times.

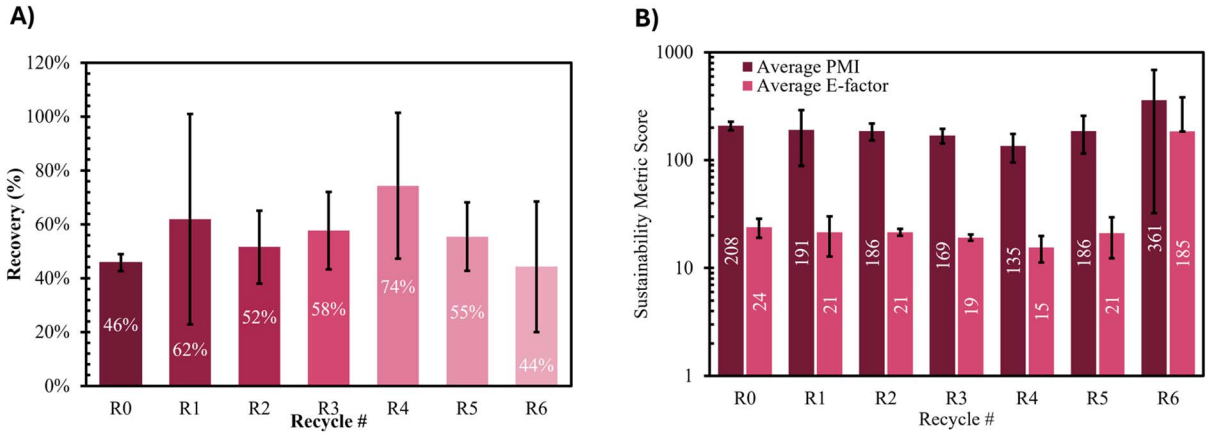

Fig. 7 Particles were made with myristic acid, 100 rpm, 70 °C thermal polymerization. (A) Recovery of PEG-DA(575) particles collected after recycles R0, R2, R4, and R6 for Trial 1 and Trial 2. Furthermore, in (B) an average sustainability metric score between Trials 1 and 2 for the initial experiment and recycles 2, 4 and 6. The full set of data can be found in the SI for recycles 0 through 6, denoted R0–R6.

recycle set after syringe filtering, which showed similar particle sizes when myristic acid was recycled. Over the 6 recycle stages, the particles retained similar size, on average 156.1 ± 85.6 nm with a PDI of 0.27 ± 0.02. Recycle 4 showed slightly larger particles, which may be a result of some myristic acid being retained in the sample or due to a larger number of particles recovered from prior trials trapped in the oil which may have undergone some degradation. Fig. S10 in the SI provides all the DLS and hydrodynamic diameter results for each oil recycling step for particles after syringe filtering and for resuspended particles post-lyophilization.

To further confirm the particles' size, SEM was used to image R2, R4, and R6 particles for Trial 1. Fig. 6 shows spherical-like particles, and many aggregates which the authors believe is due to the presence of myristic acid. The average particle sizes for pristine myristic acid (R0) and four times recycled oil (R4) were not statistically significant at 314.6 ± 295.6 nm and 300.9 ± 236.1 nm, respectively ($t(99)$, $p = 0.72$). However, the sixth recycle step, where the process was stopped, resulted in the average particle size increasing to 417.3 ± 149.9 nm ($t(99)$, R2–R6$p = 0.002$, R4–6 $p < 0.001$). This could be related to the increase in water content of the myristic acid phase by altering the oil-to-water ratio and creating larger particles. The increase of water in the oil phase was determined by DSC where a decrease in crystallinity is seen with each myristic acid reuse as shown in SI Fig. S12. An increase in water peak was also seen in the FTIR which is also shown in SI Fig. S11. Additionally, it appears that the degree of nanoparticle aggregation decreases as the oil is recycled which the authors believe is a result of more effective washing procedure.

In addition to validating particle sizes, recovery of the nanoparticles is an important metric. The recovery, shown in Fig. 7A, had a larger variability during the recycling which may be related to recovery of lingering PEG nanoparticles trapped in the myristic acid upon its recrystallization. These particles can be recovered during other subsequent stages, and we noted that the purity of particles through recycling stays approximately the same as seen in Fig. S17.

To confirm the positive impact of recycling on the sustainability metrics, *E*-factor and PMI were calculated for the different oil recycling steps. As previously discussed, the efficiency of the process can be evaluated by calculating the Process Mass Index (PMI) using eqn (6), which accounts for all reagents and solvents. The average PMI for Recycles 0, 2, 4 and 6 are reported in Fig. 7B. In Fig. 7B, there is an observed decrease in PMI at each recycling stage, until Recycle 5 (PMI = 211.0) due to the accumulation of water in the oil phase. We hypothesize that the amount of water can be dropped by further drying or reheating of the oil to force the macroscopic phase separation. The overall average PMI, calculated using eqn (7), for the initial synthesis (R0) with five additional oil recycling stages (R1–R5), was 173.4 ± 56.1. Using eqn (8), the average *E*-factor for each individual recycling stage remained under 30, as seen in Fig. 7B. Furthermore, the average *E*-factor for Recycle 5 was 21.0, remaining within the range observed for the previous recycling stages, unlike what was observed for the PMI. Using eqn (9) the average *E* factor (which does not include water as a material) for recycle 1 through 5 was below 19.7 ± 5.5, with the sixth recycle and final synthesis in this study, considering myristic acid as waste. Compared to other hydrogel synthesis techniques at the laboratory scale previously mentioned, the method presented in this paper reduces the waste generated per cycle and improves synthesis techniques used in the nanoparticle synthesis field.

Enzymatic encapsulation by proposed method

Polymer particles have been proposed to deliver enzymes to the body or to create materials with enhanced responsiveness to swelling agent composition.[66,67] Enzymes can have different stability under the synthesis conditions necessary for the creation of nanoparticles which means that synthesis methods need to be evaluated for their impact on enzyme activity. Lipases have poor thermal stability, thus the high temperature required in this method would potentially lead to complete deactivation of

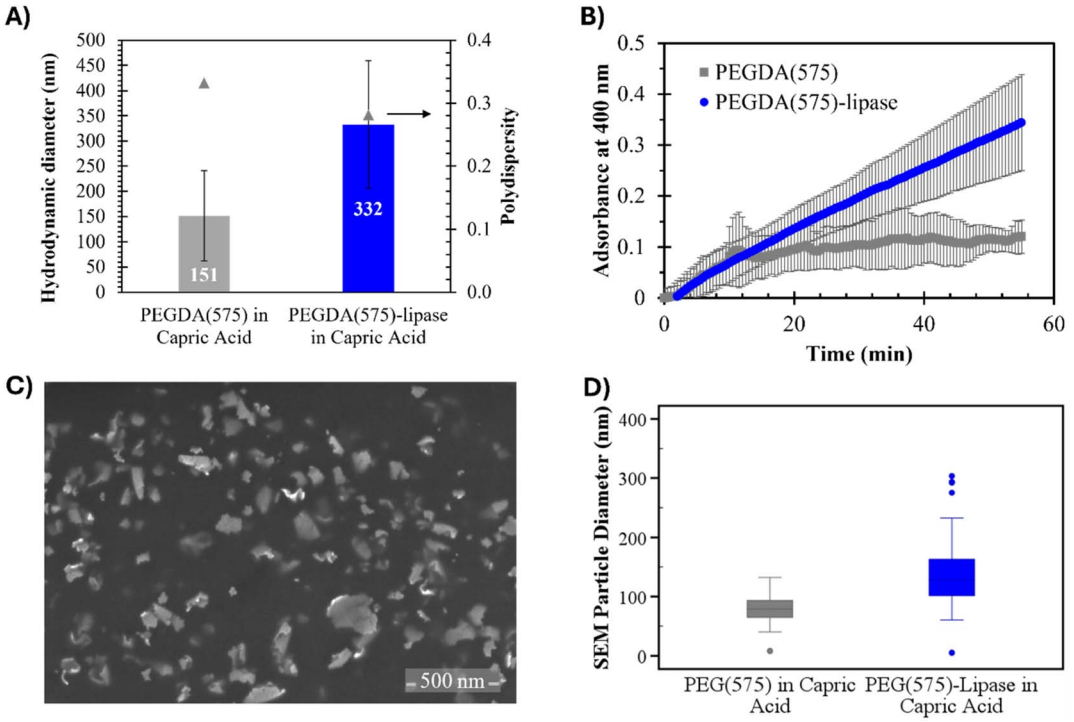

Fig. 8 Encapsulation of lipase in PEG-DA(575) nanogels synthesized in capric acid and 900 rpm conditions and redox polymerization. (A) The hydrodynamic diameter was 151.5 ± 89.4 nm with a polydispersity index of 0.33 ± 0.15 for the control PEG-DA (575) ($n = 3$) and 332.4 ± 126.4 nm with a polydispersity index of 0.28 ± 0.06 for the lipase encapsulated sample ($n = 3$) post syringe filtering within two hours post synthesis. (B) The enzyme activity was assessed using *p*-nitrophenol butyrate by measuring the absorbance at 400 nm over a sixty minute period ($n = 3$). (C) SEM results of the dry polymer-enzyme particles (D) The box plot of the SEM particle sizes obtained using ImageJ reveal there is a large distribution in particle sizes is to be expected as there was aggregation due to residual oil. The resulting in particle sizes of were 78.7 ± 22.3 nm for the control lipase free sample and 117.8 ± 56.9 nm for the lipase encapsulated sample ($n = 51$, $N = 2$ for control; $n = 162$ $N = 2$ for lipase sample).

lipase upon encapsulation. Thus, to bypass this limitation, the oil types employed in this method need to be broadened.

To assess the versatility of the method with challenging substrates, a lipase-PEG hydrogel was synthesized, and the activity of the enzyme was tracked. To achieve synthesis at a lower temperature myristic acid was replaced with capric acid, a C_{10} fatty acid, which has a melting point between 29–32.3 °C.[46,47] Due to the lower temperature a redox initiator system using iron gluconate and ammonium persulfate was used.

To confirm the chemistry of the redox system, bulk gels without the lipase were synthesized. A gel was created using the protocol from Kaeek, *et al.*, which first performed a Michael addition of PEG-DA to the lipase, before the polymerization. The swelling ratio and gel fraction made with and without lipase were found to be similar at approximately a swelling ratio of 4.0 and gel fraction at 91%, SI Fig. S3. Initially, control lipase-free nanoparticles were synthesized to determine the impact of oil type on the synthesis. Overall, there was a significant decrease in particle size noted by SEM when using capric acid and redox polymerization *vs.* myristic acid and thermal polymerization which is shown in the SI. The redox polymerization at 35 °C in capric acid yielded particles with an average particle size of 78.7 ± 22.3 nm, while 70 °C in myristic acid created particles with an average particle size of 393.6 ± 188.4 nm. This significant difference in average particle size may be due to the higher viscosity of capric acid than myristic acid, which is correlated with smaller particle sizes. This finding is supported by prior experiments at elevated temperatures with variable initiator types, noting only a small changes in particle size.

Using established W/O techniques per our recrystallization separation method, the porcine pancreas lipase was encapsulated in PEG-DA(575) nanogels using the redox polymerization described in this section. Fig. 8A provides the DLS particle size, revealing similar particle sizes seen using capric acid. The hydrodynamic diameter was 151.5 ± 89.4 nm with a PDI of 0.23 ± 0.01 and there is no statistically significant difference in sizes when lipase was incorporated *vs.* the control ($t(5)$, $p = 0.11$). In some samples, there exists a second peak that is larger than the syringe filter pore size of 1.2 μm, which could be residual capric acid that has aggregated after resuspension of lipase-containing particles. The particle sizes were further confirmed using SEM analysis, shown in Fig. 8C. First, the particles' shape is non-spherical and flaky. Irregular hydrogel morphologies comparable to those reported here, have also been described in protein-based emulsion gels, where proteins at higher volume fractions, drive droplet coalescence and fibril or network-like structures.[68,69] Furthermore, interfacial proteins can change droplet shape, gel microstructure and rheology, which can lead to non-spherical particles. The average particle sizes found using ImageJ were 117.8 ± 56.9 nm using lipase.

The recovery of PEG-DA(575)-lipase was 13.0 ± 3.1%, while the experiments with capric acid only recovered 23.2 ± 10.8%

before ethanol washing. Post-ethanol washing, the recovery of the sample dropped by approximately 8% as the fatty acids were washed away. Possible causes for low recovery may be attributed to some particles being trapped in the oil as the oil layer was not washed to extract additional particles. Additionally, the bulk gel created using the same redox polymerization method with the lipase revealed a swelling ratio of $\sim 4.70 \pm 0.08$ with a gel fraction of 0.69 ± 0.04. The swelling ratio was similar to that of PEG-DA, suggesting the network density was not impacted by lipase. However, the reduction in gel fraction indicated that not all the polymer or lipase was not incorporated into the network.

To determine if the enzyme activity is retained through crosslinking, lipase activity was assessed by using *p*-nitrophenyl butyrate. As noted in Fig. 8B, the change in absorbance is linear and continues to increase, which is expected as the enzyme continues to hydrolyze *p*-nitrophenyl butyrate.[69] As lipase solubility is limited in water, our loading was relatively low to not impact particle formation. Additionally, our process of filtering insoluble components post incubation with PEG-DA may lead to different enzyme concentration in each replicate as the solution is really heterogenous. Qualitatively we can conclude that our encapsulation efficiency remains relatively high by observing enzyme activity before polymerization and after as seen in Fig. S16. Further studies can explore different enzymes or other temperature sensitive cargo which can be encapsulated with this method.

Conclusions

Herein, a water-in-oil nanoemulsion technique that used thermally driven separation to obtain solid–liquid separation for the improvement in sustainability of nanoparticle synthesis is described. Using PEG-DA(8000) with a stirring speed of 900 rpm, the average particle size was 72.1 ± 20.56 nm using SEM and 149.6 ± 83.2 nm using DLS. The particles were uniform in shape, with a narrow size distribution. However, upon lowering the molecular weight, there was a broader distribution of particle sizes due to a decrease in viscosity, leading to aggregates of PEG-DA(575) particles, and an increase in hydrophobicity, thus more interactions with the oil layer causing coalescence. Additionally, it was shown that the oil layer can be recycled six times to recover PEG-DA(575) particles at the end of each cycle, with no statistically significant differences in particle sizes between recycles. These results confirm that our process has adequate reproducibility with the possibility of recycling the oil layer beyond the six times we have described here.

Adding recyclability to a process provides a positive sustainability parameter that is appealing to larger-scale production. The sustainability assessment of the proposed separation process resulted in an overall PMI and *E*-factor of 173.4 ± 56.1 and 19.7 ± 5.5, respectively. Not only is this lower than other literature values that assessed the sustainability scores for their processes, but this is also less than those found in the pharmaceutical industries. While we used myristic acid and PEG-DA to prove our process was recyclable, this process can be used for other oils that are crystalline at room temperature, and with polymers that have cross-linkable bonding groups if the macromers or monomers are primarily soluble in the aqueous phase. As evidence that this process can be replicated with another oil and different polymerization techniques, capric acid was used to synthesize PEG-DA(575) nanogels using redox polymerization at lower temperatures. Compared to those synthesized in a myristic acid emulsion, the average particle sizes and their variability were similar. Lipase enzyme was encapsulated into particles and a kinetic analysis of the enzymatic activity showed enzyme had remained stable at the synthesis conditions.

Overall, our improvement of established W/O emulsion techniques has shown good reproducibility in recovery and particle sizes, with excellent sustainability metric scores. Future studies can explore the improvement of recovery, especially for those particles involving the encompassment of biological species. Furthermore, evaluation of green techniques that can provide particles with less residual oil, would also add to the purity and appeal of our separation using recrystallization.

Experimental

Materials

Myristic acid, capric acid, poly(ethylene glycol) diacrylate (M_n = 8000) [PEG-DA(8000)], Gelatin Acrylate (300 bloom), lipase from porcine pancreas (125 unit per mg), iron gluconate, ammonium persulfate, isopropyl alcohol and reagent alcohol (90% ethanol), isopropyl alcohol, poly(ethylene glycol) diacrylate (M_n = 575) [PEG-DA(575)] and 2,2′-azobis(2-methylpropionamidine) dihydrochloride (97%) [AAPH], Tween-80, *n*-heptane, methanol ACS grade, sodium dihydrogen phosphate dihydrate (98 + %), and 1 N hydrochloric acid, were purchased from Sigma Aldrich and Thermo Fisher Scientific. Ultrapure type 1 water was taken from a Millipore Direct-Q® 3UV water purification system.

Literature inclusion for nanoparticles review

Papers were identified in PubMed database from the year 2000 until 2024 on February 18th, 2025. The papers using nanoparticles were found using a search query (nanoparticles). The papers citing concerns over nanoparticle use were found using the search query (((((((toxicity of nanoparticles)) OR (toxic nanoparticles)) OR (harmful nanoparticles)) OR (unsustainable nanoparticles)) OR (risks of nanoparticles)) OR (nanoparticle biocompatibility)) OR (nanoparticle cytotoxicity)). The papers using green or sustainable approaches were found using the following search query ((((((safe nanoparticles) OR (environmentally friendly nanoparticles)) OR (green synthesis of nanoparticles)) OR (sustainable nanoparticles)) OR (green nanoparticles)) OR (nontoxic nanoparticles).

Synthesis methods

Preparation of hydrogels in a water-in-oil emulsion. The aqueous phase, also known as the dispersed phase, for thermally initiated polymerization contains water and either PEG-DA(575) or PEG-DA(8000), and the radical initiator, AAPH. The aqueous phase was created to have 16.6 v/v% PEG-DA in water,

and 0.1 wt v^{-1}% of AAPH for a total of 4.2 mL aqueous layer. Myristic acid, as C_{14} fatty acid, (22.5 mL) was heated in aluminum beads with precision heating on a Hei-PLATE Mix 'n' Heat Expert until 55 °C and stirred using a magnetic stir bar. The impact of stirring speed was evaluated for myristic acid using 900 and 100 rpm. Varying stirring speeds allows for the investigation of the effects of shearing and if the size of the particles could be tuned as droplet breakup often occurs by mechanical energy. These stirring speeds are within the typical range of a nanoemulsion process.[31,33,45] After melting the oil layer, also known as the continuous phase, the aqueous solution was quickly added to the oil using a syringe to create a 5.4 : 1 oil: water emulsion. The beaker was covered with aluminum foil to ensure the temperature was stable and to minimize any splashing. Once the solution reached between 70–75 °C, a timer was set for one hour to allow polymerization to occur (typically 20 minutes after aqueous solution addition). After an hour, the emulsion was removed from the hot plate, and without further stirring, 70 mL of Ultrapure type 1 water at 50 °C was added to the emulsion. The solution was allowed to phase separate and cool overnight. Gelatin acrylate particles were synthesized using a 15% v/v in water, with the same thermal polymerization method as PEG-DA(575), except the aqueous layer was first heated to 50 °C to bring the gelatin to a liquid, while gently stirring. Once a liquid had formed, 0.1 wt% AAPH was added and then the aqueous layer was quickly added to myristic acid using a syringe.

To synthesize particles containing lipase or control particles without lipase, the emulsion system utilized capric acid. The aqueous phase for redox-initiated polymerization contained water, PEG-DA(575) or PEG-DA(8000), enzyme, and the redox initiator, APS, and iron gluconate. The aqueous phase, or dispersant phase, was created in two parts. The first part (A) had 16.6 v/v% PEG-DA in water, and 1.5 mM iron gluconate in 2.2 mL total volume. When the enzyme was intended to be crosslinked into the network, 100 mg (12 500 units) was added to solution A and allowed to stir for 24 hours before use. The solution was filtered through a 0.45 μm filter. Post filtration the enzyme loading dropped to 122.2 ± 8.38 units per mL. The second part (B) had 16.6 v/v% PEG-DA in water, and 0.75 mM APS in 2.2 mL total volume. Capric acid, as C_{10} fatty acid, (12.5 mL) was heated in aluminum beads with precision heating until 35 °C and stirred using a magnetic stir bar. After melting the continuous phase, the stir speed was set to 900 rpm, and the two water solutions (solution A and B) were added quickly to the oil using individual syringes to create a 5.4 : 1 oil: water emulsion. The beaker was covered with aluminum foil to ensure the temperature was stable and to minimize any splashing. After polymerizing for 5 minutes, 20 mL of Ultrapure type 1 water was added to the emulsion, which was then removed from the hot plate. The solution was allowed to separate and cool overnight at room temperature in the fume hood.

Purification of hydrogel nanoparticles. Upon cooling overnight, two distinct layers were observed regardless of the oil type, and the recrystallized oil layer was carefully removed from the top of the water layer using a spatula. Although much of the recrystallized oil could be removed in a single separation step, some residual crystals remained. Vacuum filtration using a 2.7 μm Whatman filter paper, followed by a 1.2 μm cellulose acetate (Sterlitech) syringe filter. The water layer was separated into centrifuge tubes and frozen for lyophilization. Using a Labconco Benchtop Freeze Dryer for 48 hours, the water was removed to isolate the particles. After lyophilization, PEG-DA(575) based particles required further purification with six reagent alcohol washes for SEM analysis using 15 mg mL^{-1} target particle concentration during each wash. Each wash was completed by centrifuging (Eppendorf 5810R) the solution at ~4288 rpm (2900×*g*)for 10 minutes, decanting, and adding more ethanol. After the final wash, the particles were dried under reduced pressure. PEG-DA(8000) based particles did not require any further purification steps after lyophilization.

Recovery of hydrogel nanoparticles. Particle yield was calculated by weighing the particles post-lyophilization and using the initial polymer mass added to the emulsion. The mass of other components utilized during synthesis were not taken into consideration when calculating the recovery of dried nanogels.

$$\text{Percent recovery}(\%) = \frac{\text{Mass of dried nanogel}}{\text{Mass of polymer used}} \times 100\% \quad (1)$$

Recycling of the myristic acid using PEG-DA(575). To reuse the myristic acid in future synthesis, the solid myristic acid sample was separated using filtration post particle synthesis protocol. The recovered myristic acid was dried overnight in the fume hood in an open top beaker at room temperature. The fume hood maintained at least 24 meters per minute. Before reusing, the oil was weighed to assess if there was any significant loss of oil from prior synthesis. If the myristic acid weight did not match the previous amount, additional pristine myristic acid was added to achieve a target weight to ensure a constant water to oil ratio. After addressing the weight of myristic acid, the same procedure was used as described above for each cycle where the recycled myristic acid was loaded into a beaker, melted, and emulsified with a water phase to produce particles.

Characterization methods

Scanning electron microscopy (SEM) and dynamic light scattering (DLS). To obtain the hydrodynamic diameter, an Anton Paar Litesizer 500 Dynamic Light Scattering (DLS) system was used, with backscattering and a disposable cuvette. Each particle sample was suspended in Type 1 Ultrapure water, using a concentration of 10 mg mL^{-1}. To confirm the sizes of the particles, an FEI Helios Nanolab 660 was used for Scanning Electron Microscopy (SEM) at 15 000× magnification. A 2 μL aliquot of the suspended samples was pipetted onto a silicon wafer and allowed to dry overnight. Before imaging, each wafer was coated with a 4.5 nm thick coating of platinum, using a sputter coater. For each sample assessed, 100–200 particle sizes were analyzed using ImageJ. Statistical analysis was carried out using Student's *t*-test ($p < 0.05$).

Swelling studies. The swelling studies for both PEG-DA(8000) and PEG-DA(575) were carried out using the gravimetric

method. For both molecular weights, 16.6 v/v% PEG-DA was crosslinked using 0.1 wt v^{-1}% AAPH at 70 °C for one hour to be consistent with the emulsion reaction time. For the redox system, only PEG-DA(575) was used at a 16.6 v/v% with 1.5 mM iron gluconate and 0.75 mM APS crosslinked for 5 minutes. The gels were first dried using a vacuum oven overnight. The weight of the dried gels was recorded and then the samples were swollen and dialyzed three times in water. The following day, the hydrogels were removed and weighed. Finally, the gels were placed back into the vacuum oven at room temperature to be dried overnight. The swelling ratio was calculated using the equation for a crosslinked polymer below:[70,71]

$$\text{Swelling ratio} = \frac{W_w - W_d}{W_d} \quad (2)$$

where W_w is the mass of the hydrated sample and W_d is the mass of the final dried sample post swelling/dialysis.

Gel fraction. To quantify the degree of crosslinking, the gel fraction was determined by creating hydrogels using PEG-DA(575), PEG-DA(8000), and PEG(575) with lipase from porcine pancreas. The hydrogels were dried *in vacuo* at room temperature in a well plate to record the initial dry weight. Each sample was then submerged in one mL of DI water for two hours. After a water exchange, one mL of fresh DI water was added, and the gels soaked for three more hours. After a final water exchange, the gels were soaked overnight. Finally, the gels were dried overnight in a vacuum oven, at room temperature and the final dry weight was recorded. The gel fraction was calculated using the following equation,

$$\text{Gel fraction} = \frac{DM_{final}}{DM_{initial}} \times 100\% \quad (3)$$

where $DM_{initial}$ is the initial dry mass of the hydrogel before commencing dialysis, and DM_{final} is the final mass after drying overnight.

NMR. To analyze whether any myristic acid remained in the samples, a 400 MHz Bruker Spectrometer was used to obtain a ^{1}H Nuclear Magnetic Resonance (NMR). The samples were suspended in 1 mL of chloroform-*d* and the spectra were analyzed using Bruker Topspin. The peaks at 1.5 ppm were noted to indicate the presence of myristic acid and 3.5 ppm to confirm the presence of PEG. Tetrahydrofuran was used as an internal standard.

DSC. Differential scanning calorimetry (DSC) was used to determine the thermal properties of the myristic acid throughout the recycling process using TA Instruments DSC 250. To test each sample, the myristic acid was dried in the fume hood at room temperature and a small aliquot was placed in an aluminum *T*-zero hermetic sample pan and sealed with a *T*-zero hermetic lid. Samples were heated from 30 °C to 90 °C at a rate of 5 °C min^{-1}, cooled to 30 °C at 5 °C min^{-1}, and then reheated to 90 °C at 5 °C min^{-1}. Analysis was conducted on the second heating cycle. Enthalpy of melting was calculated by integrating the endothermic peak. The percentage of crystallinity was calculated assuming the pristine myristic acid samples were 100% crystalline. Furthermore, the equation used to calculate the percent crystallinity, χ_c is below:

$$X_C = \frac{\Delta H_m}{\Delta H_o} \times 100\% \quad (4)$$

where ΔH_m is the enthalpy of melting of myristic acid after the process, and ΔH_0 is the enthalpy of pristine myristic acid, both obtained from the peak integration function within TA Instrument's TRIOS DSC software.

HPLC. High Performance Liquid Chromatography (HPLC) was utilized to assess the purity of PEG-DA(575) nanogels during the recycling of myristic acid and of gelatin acrylate after redox polymerization. Following water removal utilizing lyophilization, 20 mg of each sample was mixed with 90 : 10 methanol and phosphate buffer adjusted to pH 2.5 for 72 hours to extract any myristic acid. To ensure PEG-DA was removed prior to analysis, the samples were passed through a 0.1 μm PVDF syringe filter. An Agilent system consisting of a 1260 Infinity isocratic pump, degasser, and temperature-controlled column chamber set to 30 °C was paired with an InfinityLab Poroshell 120 EC-C18, 3.0 × 100 mm, 4 μm column. The mixture of 90 : 10 methanol and phosphate buffer served as the mobile phase at 0.5 mL min^{-1}. A calibration curve of pure myristic acid at concentrations of 10, 5, 2.5, 1.25, 0.625, and 0.3125 mg mL^{-1} was created to quantify myristic acid remaining after synthesis utilizing solid–liquid separation. Detection was achieved with Wyatt Technologies detectors through differential refractive index *via* an Optilab TrEX.

Enzyme activity

Enzyme activity was assessed using a *p*-nitrobutyrate. A Greiner 96-well acrylic plate was used in a BioTek Synergy H1 multimode microplate reader. 1 mg of particles was suspended in 100 μL of phosphate buffered saline. 50 mM *p*-nitrophenol butyrate isopropyl alcohol solution was prepared and 2 μL were pipetted into each well. Free enzyme was suspended in water and filtered through a 1.2 μm filter and also added tested with the same loading of reagents to mimic the particle formation process. The absorbance was monitored for sixty minutes at time intervals of 30 seconds. To analyze the enzymatic activity of our particles. The absorbance was plotted *versus* time and Beer's law was used to confirm the concentration of the *p*-nitrophenol in the solution at 400 nm. A molar extinction coefficient of 12 800 M^{-1} cm^{-1} was used.[72]

Ohnesorge and Weber scaling factor

The scaling factor was calculated using eqn (5) from work by Gupta *et al.*[45] The ratio involves viscosity of the disperse phase (aqueous phase) to the continuous phase viscosity (oil phase)

$$d = 171 \times \left(\frac{\mu_d^{\frac{1}{3}}}{\mu_c^{-\frac{5}{12}}} \right) \quad (5)$$

Sustainability metric scores

Sustainability metrics for the synthesis were calculated first using process mass intensity (PMI) described in eqn (6) and the overall average PMI for the recycling stages was determined by eqn (7). Throughout the process, the mass of all reagents, products, and waste were tracked.

$$\text{PMI} = \frac{\text{Total mass in a process or process step(g)}}{\text{Mass of product(g)}} \quad (6)$$

$$\text{Overall average PMI} = (\sum\text{PMI R1 through R5 in (Trial 1 + Trial 2 + Trial 3))/15} \quad (7)$$

Furthermore, *E*-factor was also calculated according to eqn (8) and the overall average *E*-factor for the recycling stages was calculated utilizing eqn (9). For this calculation, the mass of water was excluded.

$$E\text{-factor} : \frac{\text{Total waste mass (g)}}{\text{Product mass(g)}} \quad (8)$$

$$\text{Overall average } E\text{-factor} = (\sum E\text{-factor R1 through R5 in (Trial 1 + Trial 2 + Trial 3))/15} \quad (9)$$

Safety

In this work, we aimed to adhere to the principles of green chemistry to eliminate or minimize hazards and waste; however, they could not be removed entirely. In particle synthesis, reactive chemicals such as PEG-DA are utilized which can be an irritant. To perform radical polymerization, a radical initiator was necessary. AAPH was used due to its water-soluble nature; however, AAPH is a spontaneously combustible solid. Additionally, AAPH has acute oral toxicity and serious eye damage and eye irritation. Ammonium persulfate, part of our redox initiation system, is an oxidant with acute toxicity and respiratory sensitizer. The risk of the chemical can be mitigated by weighing the solid materials in a fume hood and making a stock solution which can be more easily manipulated. It is worth noting that stock solutions in our study were used within approximately 24–48 hours of creation to minimize any loss of reactivity, particularly in our redox system.

Author contributions

The manuscript was written through the contributions of all authors. All authors have approved the final version of the manuscript. Emily Ingram: investigation, methodology, visualization, writing – original draft, writing – review & editing. Jason Stallings, Jr.: investigation, writing – review & editing. Mara Leach: investigation, writing – review & editing. Endras Fadhilah- investigation, writing – review & editing. Anastasia Shaverina: investigation, methodology, writing – review & editing. Brittany E. Givens: conceptualization, writing – review & editing. Malgorzata Chwatko: conceptualization, validation, methodology, supervision, visualization, writing – original draft, writing – review & editing.

Conflicts of interest

There are no conflicts to declare.

Abbreviations

PEG-DA	Poly(ethylene glycol) diacrylate
APS	Ammonium persulfate
AAPH	2,2′-Azobis(2-methylpropionamidine) dihydrochloride (97%)
NMR	Nuclear magnetic resonance
DLS	Dynamic light scattering
SEM	Scanning electron microscopy
HPLC	High performance liquid chromatography

Data availability

Data for this article, including raw data from DSC, SEM, NMR are available at Open Science Framework repository at https://osf.io/gazrc/overview?view_only=9406d83cfb3a47dd9d51369b4d0f3713.

Supplementary information: the document includes additional DLS characterization, comparison to *n*-heptane as a solvent for particle synthesis, hydrogel swelling and gel fraction characterization. See DOI: https://doi.org/10.1039/d5ra07694c.

Acknowledgements

Funding was provided by the University of Kentucky. This work was performed in part at the U.K. Electron Microscopy Center, a member of the National Nanotechnology Coordinated Infrastructure (NNCI), which is supported by the National Science Foundation (NNCI-2025075). We would like to thank Nico Briot for his assistance with the SEM image collection. We would like to acknowledge the use of the Nuclear Magnetic Resonance (NMR) Center in the College of Arts and Sciences at the University of Kentucky. Scheme created in BioRender. Ingram, E. (2025) https://BioRender.com/y89c256.

References

1 S. Ying, Z. Guan, P. C. Ofoegbu, P. Clubb, C. Rico, F. He and J. Hong, Green synthesis of nanoparticles: Current developments and limitations, *Environ. Technol. Innovat.*, 2022, **26**, 102336, DOI: 10.1016/j.eti.2022.102336.

2 Y. Herdiana, N. Wathoni, S. Shamsuddin and M. Muchtaridi, Scale-up polymeric-based nanoparticles drug delivery systems: Development and challenges, *OpenNano*, 2022, **7**, 100048, DOI: 10.1016/j.onano.2022.100048.

3 H. Duan, D. Wang and Y. Li, Green chemistry for nanoparticle synthesis, *Chem. Soc. Rev.*, 2015, **44**(16), 5778–5792, DOI: 10.1039/c4cs00363b.

4 J. Singh, T. Dutta, K. H. Kim, M. Rawat, P. Samddar and P. Kumar, Green' synthesis of metals and their oxide

nanoparticles: applications for environmental remediation, *J. Nanobiotechnology*, 2018, **16**(1), 84, DOI: 10.1186/s12951-018-0408-4.

5 J. Martínez, J. F. Cortés and R. Miranda, Green Chemistry Metrics, A Review, *Processes*, 2022, **10**(7), 1274, DOI: 10.3390/pr10071274.

6 A. S. El-Kalliny, M. S. Abdel-Wahed, A. A. El-Zahhar, I. A. Hamza and T. A. Gad-Allah, Nanomaterials: a review of emerging contaminants with potential health or environmental impact, *Discover Nano*, 2023, **18**(1), 68, DOI: 10.1186/s11671-023-03787-8.

7 W. Najahi-Missaoui, R. D. Arnold and B. S. Cummings, Safe Nanoparticles: Are We There Yet?, *Int. J. Mol. Sci.*, 2020, **22**(1), 385, DOI: 10.3390/ijms22010385.

8 S. J. Rukmani, P. Lin, J. S. Andrew and C. M. Colina, Molecular Modeling of Complex Cross-Linked Networks of PEGDA Nanogels, *J. Phys. Chem. B*, 2019, **123**(18), 4129–4138, DOI: 10.1021/acs.jpcb.9b01622.

9 Q. Feng, D. Li, Q. Li, X. Cao and H. Dong, Microgel assembly: Fabrication, characteristics and application in tissue engineering and regenerative medicine, *Bioact. Mater.*, 2022, **9**, 105–119, DOI: 10.1016/j.bioactmat.2021.07.020.

10 B. V. N. Nagavarma, H. Yadav, A. Ayaz, L. S. Vasugha and H. G. Shivakumar, Different techniques for preparation of polymeric nanoparticles- A review, *Asian J. Pharm. Clin. Res.*, 2012, **5**(3), 16–23.

11 S. P. Zustiak and J. B. Leach, Hydrolytically Degradable Poly(ethylene Glycol) Hydrogel Scaffols with Tunable Degradation and Mechanical Properties, *Biomacromolecules*, 2010, **11**, 1348–1357.

12 M. Levin, Y. Tang, C. D. Eisenbach, M. T. Valentine and N. Cohen, Understanding the Response of Poly(ethylene glycol) diacrylate (PEGDA) Hydrogel Networks: A Statistical Mechanics-Based Framework, *Macromolecules*, 2024, **57**(15), 7074–7086, DOI: 10.1021/acs.macromol.3c02635.

13 Y. Wang, S. Zhang and D. S. W. Benoit, Degradable poly(ethylene glycol) (PEG)-based hydrogels for spatiotemporal control of siRNA/nanoparticle delivery, *J. Control Release*, 2018, **287**, 58–66, DOI: 10.1016/j.jconrel.2018.08.002.

14 M. Parlato, S. Reichert, N. Barney and W. Murphy, Poly(ethylene glycol) Hydrogels with Adaptable Mechnical Degradation Properties for Use in Biomedical Applications, *Macromol. Biosci.*, 2014, **14**(5), 687–698.

15 F. Kawai, *Biodegradation of Polyethers (Polyethylene Glycol, Polypropylene Glycol, Polytetramethylene Glycol, and Others)*, A. Steinbüchel, 2005, DOI: 10.1002/3527600035.bpol9012.

16 I. Bjornsdottir, O. Sternebring, W. A. Kappers, H. Selvig, H. T. Korno, J. B. Kristensen and M. A. Bagger, Pharmacokinetics, tissue distribution and excretion of 40kDa PEG and PEGylated rFVIII (N8-GP) in rats, *Eur. J. Pharm. Sci.*, 2016, **87**, 58–68, DOI: 10.1016/j.ejps.2015.10.020.

17 C. S. A. Lima, T. S. Balogh, J. Varca, G. H. C. Varca, A. B. Lugao, A. C.-C. L, E. Bucio and S. S. Kadlubowski, An Updated Review of Macro, Micro, and Nanostructured Hydrogels for Biomedical and Pharmaceutical Applications, *Pharmaceutics*, 2020, **12**(10), 970, DOI: 10.3390/pharmaceutics12100970.

18 M. Y. Koroleva and E. V. Yurtov, Ostwald ripening in macro- and nanoemulsions, *Russ. Chem. Rev.*, 2021, **90**(3), 293–323, DOI: 10.1070/rcr4962.

19 L. Qiao and M. T. Swihart, Solution-phase synthesis of transition metal oxide nanocrystals: Morphologies, formulae, and mechanisms, *Adv. Colloid Interface Sci.*, 2017, **244**, 199–266, DOI: 10.1016/j.cis.2016.01.005.

20 H. Jiang, Y. Sheng and T. Ngai, Pickering emulsions: Versatility of colloidal particles and recent applications, *Curr. Opin. Colloid Interface Sci.*, 2020, **49**, 1–15, DOI: 10.1016/j.cocis.2020.04.010.

21 S. N. Kale and S. L. Deore, Emulsion Micro Emulsion and Nano Emulsion: A Review, *Sys. Rev. Pharm.*, 2016, **8**(1), 39–47, DOI: 10.5530/srp.2017.1.8.

22 A. Chebil, J. Desbrières, C. Nouvel, J.-L. Six and A. Durand, Ostwald ripening of nanoemulsions stopped by combined interfacial adsorptions of molecular and macromolecular nonionic stabilizers, *Colloids Surf., A*, 2013, **425**, 24–30, DOI: 10.1016/j.colsurfa.2013.02.028.

23 D. Prat, A. Wells, J. Hayler, H. Sneddon, C. R. McElroy, S. Abou-Shehada and P. J. Dunn, CHEM21 selection guide of classical- and less classical-solvents, *Green Chem.*, 2016, **18**(1), 288–296, DOI: 10.1039/c5gc01008j.

24 M. S. Rehmann, K. M. Skeens, P. M. Kharkar, E. M. Ford, E. Maverakis, K. H. Lee and A. M. Kloxin, Tuning and Predicting Mesh Size and Protein Release from Step Growth Hydrogels, *Biomacromolecules*, 2017, **18**(10), 3131–3142, DOI: 10.1021/acs.biomac.7b00781.

25 Z. Zhang, D. W. Grijpma and J. Feijen, Poly(trimethylene carbonate) and monomethoxy poly(ethylene glycol)-block-poly(trimethylene carbonate) nanoparticles for the controlled release of dexamethasone, *J. Control Release*, 2006, **111**(3), 263–270, DOI: 10.1016/j.jconrel.2005.12.001.

26 B. V. N. Nagavarma, K. S. Y. Hemant, A. Ayaz, L. S. Vasugha and H. G. Shivakumar, Different Techniques for Preparation of Polymeric Nanoparticles- A Review, *Asian J. Pharmaceut. Clin. Res.*, 2012, **5**, 16–23.

27 H. Bhardwaj and R. K. Jangde, Current updated review on preparation of polymeric nanoparticles for drug delivery and biomedical applications, *Next Nanotechnol.*, 2023, **2**, 100013, DOI: 10.1016/j.nxnano.2023.100013.

28 M. E. Abdel-Raouf, S. M. El-Saeed, E. G. Zaki and A. M. Al-Sabagh, Green chemistry approach for preparation of hydrogels for agriculture applications through modification of natural polymers and investigating their swelling properties, *Egypt. J. Pet.*, 2018, **27**(4), 1345–1355, DOI: 10.1016/j.ejpe.2018.09.002.

29 P. Bhardwaj, B. Singh and S. P. Behera, Green approaches for nanoparticle synthesis: emerging trends, *Nanomaterials*, 2021, 167–193.

30 R. Sánchez, J. M. Franco, M. A. Delgado, C. Valencia and C. Gallegos, Development of new green lubricating grease formulations based on cellulosic derivatives and castor oil, *Green Chem.*, 2009, **11**(5), 686–693, DOI: 10.1039/b820547g.

31 S. Akram, N. Anton, Z. Omran and T. Vandamme, Water-in-Oil Nano-Emulsions Prepared by Spontaneous Emulsification: New Insights on the Formulation Process, *Pharmaceutics*, 2021, **13**(7), 1030, DOI: 10.3390/pharmaceutics13071030.

32 A. L. Radu, A. M. Gavrila, B. Cursaru, C. P. Spatarelu, T. Sandu, A. Sarbu, M. Terodorescu, F. X. Perrin, T. V. Iordache and A. Zaharia, Poly(ethylene Glycol) Diacrylate-Nanogels Synthesized by Mini-emulsion Polymerization, *Mater. Plast.*, 2019, **56**(3), 514–519.

33 M. A. Aravand and M. A. Semsarzadeh, Particle Formation by Emulsion Inversion Method: Effect of the Stirring Speed on Inversion and Formation of Spherical Particles, *Macromol. Symp.*, 2008, **274**(1), 141–147, DOI: 10.1002/masy.200851419.

34 S. R. Tipson, Theory, Scope, and Methods of Recrystallization, *Anal. Chem.*, 1950, **22**, 628–636, DOI: 10.1021/ac60041a002.

35 B. L. C. Cunha, J. O. Bahu, L. F. Xavier, S. Crivellin, S. D. A. de Souza, L. Lodi, A. L. Jardini, R. M. Filho, M. Schiavon, V. O. C. Concha, P. Severino and E. B. Souto, Lactide: Production Routes, Properties, and Applications, *Bioengineering*, 2022, **9**(4), 164, DOI: 10.3390/bioengineering9040164.

36 N. Doshi, B. Demeule and S. Yadav, Understanding Particle Formation: Solubility of Free Fatty Acids as Polysorbate 20 Degradation Byproducts in Therapeutic Monoclonal Antibody Formulations, *Mol. Pharm.*, 2015, **12**(11), 3792–3804, DOI: 10.1021/acs.molpharmaceut.5b00310.

37 J. B. Aswathanarayan and R. R. Vittal, Nanoemulsions and Their Potential Applications in Food Industry, *Front. Sustain. Food Syst.*, 2019, **3**, 95, DOI: 10.3389/fsufs.2019.00095.

38 T. Zhang, F. Liu, J. Wu and T. Ngai, Pickering emulsions stabilized by biocompatible particles: A review of preparation, bioapplication, and perspective, *Particuology*, 2022, **64**, 110–120, DOI: 10.1016/j.partic.2021.07.003.

39 M. Zembyla, B. S. Murray and A. Sarkar, Water-in-oil emulsions stabilized by surfactants, biopolymers and/or particles: a review, *Trends Food Sci. Technol.*, 2020, **104**, 49–59, DOI: 10.1016/j.tifs.2020.07.028.

40 M. L'Estime, M. Schindler, N. Shahidzadeh and D. Bonn, Droplet Size Distribution in Emulsions, *Langmuir*, 2024, **40**(1), 275–281, DOI: 10.1021/acs.langmuir.3c02463.

41 Y. Hamzah, W. M. Z. W. Yunus, N. M. Isa, R. Tajau, K. Hashim and K. Z. Dahlan, Synthesis of polyethylene glycol diacrylate nanogel using irradiation of inverse micelles technique, *e-Polymers*, 2012, **12**(1), 45, DOI: 10.1515/epoly.2012.12.1.533.

42 M. Nazari, M. A. Mehrnia, H. Jooyandeh and H. Barzegar, Preparation and characterization of water in sesame oil microemulsion by spontaneous method, *J. Food Process. Eng.*, 2019, **42**(4), e13032, DOI: 10.1111/jfpe.13032.

43 H. Park, Exploring the Effects of Process Parameters during W/O/W Emulsion Preparation and Supercritical Fluid Extraction on the Protein Encapsulation and Release Properties of PLGA Microspheres, *Pharmaceutics*, 2024, **16**(3), 302, DOI: 10.3390/pharmaceutics16030302.

44 M. Saghaei, E. R. Fotsing, A. Ross and L. Fradette, Production of Monodisperse Large Drop Emulsions by Means of High Internal Phase Pickering Emulsions-Processing and Formulation, *Ind. Eng. Chem. Res.*, 2024, **63**(42), 17917–17929, DOI: 10.1021/acs.iecr.4c01855.

45 A. Gupta, H. B. Eral, T. A. Hatton and P. S. Doyle, Controlling and predicting droplet size of nanoemulsions: scaling relations with experimental validation, *Soft Matter*, 2016, **12**(5), 1452–1458, DOI: 10.1039/c5sm02051d.

46 M. Majo, R. Sanchez, P. Barcelona, J. Garcia, A. I. Fernandez and C. Barreneche, Degradation of Fatty Acid Phase-Change Materials (PCM): New Approach for Its Characterization, *Molecules*, 2021, **26**(4), 982, DOI: 10.3390/molecules26040982.

47 N. B. Matcha, K. K. Sahu and B. D. Pandey, Zinc recovery from sphalerite concentrate by direct oxidative leaching with ammonium, sodium and potassium persulphates, *Hydrometallurgy*, 2002, **64**, 119–129, DOI: 10.1016/S0304-386X(02)00030-0.

48 Z. Zhang, Y. Yuan, N. Zhang and X. Cao, Experimental investigation on thermophysical properties of capric acid–lauric acid phase change slurries for thermal storage system, *Energy*, 2015, **90**, 359–368, DOI: 10.1016/j.energy.2015.06.129.

49 W. Deng, Y. Yan, P. Zhuang, X. Liu, K. Tian, W. Huang and C. Li, Synthesis of nanocapsules blended polymeric hydrogel loaded with bupivacaine drug delivery system for local anesthetics and pain management, *Drug Deliv.*, 2022, **29**(1), 399–412, DOI: 10.1080/10717544.2021.2023702.

50 L. Perrin, S. Desobry-Banon, G. Gillet and S. Desobry, Phase Diagram of Pickering Emulsions Stabilized by Cellulose Nanocrystals, *Polymers*, 2023, **15**(13), 2783, DOI: 10.3390/polym15132783.

51 P. A. Lovell and F. J. Schork, Fundamentals of Emulsion Polymerization, *Biomacromolecules*, 2020, **21**(11), 4396–4441, DOI: 10.1021/acs.biomac.0c00769.

52 S.-R. Yun, G.-O. Kim, C. W. Lee, N.-J. Jo, Y. Kang, K.-S. Ryu and L. A. F. Coelho, Synthesis and Control of the Shell Thickness of Polyaniline and Polypyrrole Half Hollow Spheres Using the Polystyrene Cores, *J. Nanomater.*, 2012, **2012**(1), 894539, DOI: 10.1155/2012/894539.

53 X. Li, Y. Huang and Y. Dan, Synthesis of sub-100 nm PMMA nanoparticles initiated by ammonium persulfate/ascorbic acid in acetone-water mixture, *Colloid Polym. Sci.*, 2020, **298**(3), 225–232, DOI: 10.1007/s00396-020-04600-z.

54 S. Bednarz, A. Wesołowska-Piętak, R. Konefał and T. Świergosz, Persulfate initiated free-radical polymerization of itaconic acid: Kinetics, end-groups and side products, *Eur. Polym. J.*, 2018, **106**, 63–71, DOI: 10.1016/j.eurpolymj.2018.07.010.

55 S. Li, Z. Song, Q. Jiang and J. Wu, Facile fabrication of multifunctional underwater superoleophobicity zwitterionic coating by surface-initiated redox polymerization, *Colloids Surf., A*, 2022, **649**, 129463, DOI: 10.1016/j.colsurfa.2022.129463.

56 Y. Koshikawa and H. Goto, Magnetic Behavior of an Iron Gluconate/Polyaniline Composite, *J. Compos. Sci.*, 2021, **5**(9), 252, DOI: 10.3390/jcs5090252.
57 T.-D. Dang, Y. H. Kim, H. G. Kim and G. M. Kim, Preparation of monodisperse PEG hydrogel microparticles using a microfluidic flow-focusing device, *J. Ind. Eng. Chem.*, 2012, **18**(4), 1308–1313, DOI: 10.1016/j.jiec.2012.01.028.
58 S. Y. An, M. P. Bui, Y. J. Nam, K. N. Han, C. A. Li, J. Choo, E. K. Lee, S. Katoh, Y. Kumada and G. H. Seong, Preparation of monodisperse and size-controlled poly(ethylene glycol) hydrogel nanoparticles using liposome templates, *J. Colloid Interface Sci.*, 2009, **331**(1), 98–103, DOI: 10.1016/j.jcis.2008.11.022.
59 C. Jimenez-Gonzalez, C. S. Ponder, Q. B. Broxterman and J. B. Manley, Using the Right Green Yardstick: Why Process Mass Intensity Is Used in the Pharmaceutical Industry To Drive More Sustainable Processes, *Org. Process Res. Dev.*, 2011, **15**(4), 912–917, DOI: 10.1021/op200097d.
60 F. Roschangar, J. Li, Y. Zhou, W. Aelterman, A. Borovika, J. Colberg, D. P. Dickson, F. Gallou, J. D. Hayler, S. G. Koenig, *et al.*, Improved iGAL 2.0 Metric Empowers Pharmaceutical Scientists to Make Meaningful Contributions to United Nations Sustainable Development Goal 12, *ACS Sustain. Chem. Eng.*, 2021, **10**(16), 5148–5162, DOI: 10.1021/acssuschemeng.1c01940.
61 E. R. Monteith, P. Mampuys, L. Summerton, J. H. Clark, B. U. W. Maes and C. R. McElroy, Why we might be misusing process mass intensity (PMI) and a methodology to apply it effectively as a discovery level metric, *Green Chem.*, 2020, **22**(1), 123–135, DOI: 10.1039/c9gc01537j.
62 E. C. Sherer, A. Bagchi, B. Kosjek, K. M. Maloney, Z. Peng, S. A. Robaire, R. P. Sheridan, E. Metwally and L.-C. Campeau, Driving Aspirational Process Mass Intensity Using Simple Structure-Based Prediction, *Org. Process Res. Dev.*, 2022, **26**(5), 1405–1410, DOI: 10.1021/acs.oprd.1c00477.
63 B. T. Reid and S. M. Reed, Improved methods for evaluating the environmental impact of nanoparticle synthesisdagger, *Green Chem.*, 2016, **18**(15), 4263–4269, DOI: 10.1039/C6GC00383D.
64 T. Jin, T. Liu, S. Jiang, D. Kurdyla, B. A. Klein, V. K. Michaelis, E. Lam, J. Li and A. Moores, Chitosan nanocrystals synthesis *via* aging and application towards alginate hydrogels for sustainable drug release, *Green Chem.*, 2021, **23**(17), 6527–6537, DOI: 10.1039/d1gc01611c.
65 R. A. Sheldon, The E factor at 30: a passion for pollution prevention, *Green Chem.*, 2023, **25**(5), 1704–1728, DOI: 10.1039/d2gc04747k.
66 J. Ouyang, J. Li and C. Wu, Protein–Polymer Conjugates: Advancing Enzyme Catalysis in Synthetic Chemistry, *ChemCatChem*, 2024, **17**(2), e202401180, DOI: 10.1002/cctc.202401180.
67 I. Rivero Berti, G. A. Islan and G. R. Castro, Enzymes and biopolymers. The opportunity for the smart design of molecular delivery systems, *Bioresour. Technol.*, 2021, **322**, 124546, DOI: 10.1016/j.biortech.2020.124546.
68 R. Li, Y. Guo, A. Dong and X. Yang, Protein-based emulsion gels as materials for delivery of bioactive substances: Formation, structures, applications and challenges, *Food Hydrocoll.*, 2023, **144**, 108921, DOI: 10.1016/j.foodhyd.2023.108921.
69 C. Wan, Q. Cheng, M. Zeng and C. Huang, Recent progress in emulsion gels: from fundamentals to applications, *Soft Matter*, 2023, **19**(7), 1282–1292, DOI: 10.1039/d2sm01481e.
70 N. Sun, T. Wang and X. Yan, Synthesis and investigation of a self-assembled hydrogel based on hydroxyethyl cellulose and itsin vitroibuprofen drug release characteristics, *RSC Adv.*, 2017, **7**(16), 9500–9511, DOI: 10.1039/c6ra25355e.
71 S. Gupta and A. Bit, Rapid prototyping for polymeric gels, In *Polymeric Gels*, 2018, pp 397–439.
72 C. S. Wu, C. T. Wu, Y. S. Yang and F. H. Ko, An enzymatic kinetics investigation into the significantly enhanced activity of functionalized gold nanoparticles, *Chem Commun*, 2008, **42**, 5327–5329, DOI: 10.1039/b810889g.